INTERANNUAL VARIABILITY OF THE ATLANTIC HADLEY CIRCULATION IN BOREAL SUMMER AND ITS IMPACTS ON TROPICAL CYCLONE ACTIVITY

BY

GAN ZHANG

THESIS

Submitted in partial fulfillment of the requirements
for the degree of Master of Science in Atmospheric Sciences
in the Graduate College of the
University of Illinois at Urbana-Champaign, 2012

Urbana, Illinois

Adviser:

Professor Zhuo Wang

Abstract

An original method was developed to define the regional Hadley circulation (HC) in terms of the meridional streamfunction. The interannual variability of the Atlantic HC in boreal summer was examined using the EOF analysis. The leading mode (M1), explaining more than 45% of the variances, is associated with the intensity change of the ITCZ. M1 is significantly correlated to multiple climate factors and has strong impacts on the Atlantic tropical cyclone (TC) activity. In the positive (negative) phase of M1, the ITCZ is stronger (weaker) than normal, and more (less) TCs form over the Atlantic main development region (MDR) with a larger (smaller) fraction of storms intensifying into major hurricanes. Composite analyses showed that the large-scale conditions are more favorable for the MDR TC activity in the positive phase.

The role of tropical easterly waves in modulating the Atlantic TC activity is highlighted. In the positive phase of M1, the wave activity is significantly enhanced over the East Atlantic and the Caribbean Sea, which can be attributed to stronger coastal convection and a more unstable mean flow. In the context of the recently proposed marsupial paradigm, the frequency and structure of wave pouches were examined. In the positive phase of M1, the pouch frequency increases, and the number of pouches with a vertically coherent structure also rises significantly. A deep and vertically aligned wave pouch has been shown highly favorable for the TC formation. The HC perspective thus provides a complete dynamic framework for understanding the impacts of the different aspects of the large-scale circulation on the TC activity.

To Father and Mother

and what leads me through the storms

in this journey

Acknowledgment

This project is unimaginable without the support of my advisor, Professor Zhuo Wang, who dedicated to the numerous discussion sessions and the whole paper writing process so much. Thanks also go to Dr. Timothy J. Dunkerton for stimulating discussion. Thanks to NOAA/OAR/ESRL PSD for storing the research data and National Science Foundation for providing research funding. And finally, thanks to my beloved parents and wonderful friends, who always offer support and love, shaping me into who I am today.

TABLE OF CONTENTS

CHAPTER 1: INTRODUCTION[1]

The Hadley circulation is one of the primary components of the large-scale circulation in the tropics. It consists of two thermally direct overturning cells, in which air rises near the equator, diverts poleward near the tropopause, sinks in the subtropics and returns equatorward near the surface. Due to the Coriolis force, the upper-level poleward flow turns eastward and contributes to the subtropical westerly jet. Similarly, the equatorward flow turns westward and results in the prevailing trade winds in the lower troposphere. The northeasterly and southeasterly trade winds meet in the intertropical convergence zone (ITCZ). Associated with the ascending branch of Hadley Cells, the ITCZ is featured by a band of heavy precipitation, cyclonic relative vorticity and relatively low surface pressure. The variability of the Hadley circulation is closely related to different aspects of the tropical climate, such as the precipitation distribution, low-level convergence and relative vorticity, as well as the tropospheric humidity and vertical wind shear (VWS).

The intensity of globally averaged Hadley circulation is significantly modulated by the variations of the El Niño–Southern Oscillation (ENSO) on the interannual time scale (Oort and Yienger 1996). Recent work suggests an intensifying trend of the Hadley circulation in the past three decades (e.g., Mitas and Clement 2005; Stachnik and Schumacher 2011). Chiang et al. (2002) examined the interannual variability of the Atlantic ITCZ precipitation and suggested that the variability is mainly controlled by the meridional Sea Surface Temperature (SST) gradient of the tropical Atlantic and the anomalous Walker circulation associated with ENSO. The

[1] The work was submitted to Journal of Climate under the same title and currently is in the peer-review process. Professor Zhuo Wang served as the second author and contributed in the result analysis and paper writing.

meridional SST gradient is linked to the Atlantic Meridional Mode (AMM, Chiang and Vimont 2004), which is involved with the air-sea interaction and induces the meridional displacement of the ITCZ.

The impacts of the large-scale envrironment on the Atlantic tropical cyclone (TC) activity have been examined in the many previous studies. Shapiro (1982) showed that the lower large-scale sea-level pressure and weaker 500 hPa westerlies over the North Atlantic precede more active hurricane seasons. Gray (1984) highlighted the impacts of ENSO on the Atlantic TC frequency via the changes of the upper-level flow pattern and the associated VWS. Landsea and Gray (1992) and Gray and Landsea (1992) found a significant correlation between the June-September rainfall at western Sahel and the number of intense hurricanes. Landsea and Gray (1992) hypothesized that the enhanced TC activity is related to a weaker VWS and stronger African easterly waves (AEWs) in a wet year. Goldenberg, et al. (2001) investigated the interannual and interdecadal variability of the TC activity over the Main Development Region (MDR; 10N˚-20˚N between the coast of West Africa and Central America), and suggested that multiple climate factors cooperatively contributed to extreme active hurricane seasons. Vimont and Kossin (2007) and Kossin and Vimont (2007) showed that the AMM is correlated with a number of local dynamical variables (i.e., VWS, low-level vorticity and convergence, static stability, and sea level pressure) that cooperate to impact Atlantic TC activity.

Over the Atlantic, a majority of TCs originate from African easterly waves (AEWs) (Landsea 1993). The relationship between the AEW activity and TC activity over the Atlantic has been examined in some previous studies. Reed (1988) suggested that TC activity may be related to variability in AEW intensity. Thorncroft and Hodges (2001) showed a positive correlation between Atlantic TC activity and the 850 hPa wave activity at the West African

coast, which was further confirmed by Hopsch et al. (2007). Most of these studies, however, focused mainly on waves over West Africa. The structure and variability of the tropical easterly waves (TEWs) over the Atlantic and their relationship with TC activity are not well-understood.

Recent work by Dunkerton et al. (2009) showed that a protected region of cyclonic recirculation exists in the lower troposphere in some, but not all, easterly waves. Such a region, the so-called wave pouch, straddles the ‘‘critical latitude’’ where the wave phase speed and the mean flow speed are equal. As demonstrated by both observational diagnoses (Wang et al. 2009; Raymond and López Carrillo 2011) and numerical model simulations (Wang et al. 2010a,b; Wang 2012; Montgomery et al. 2010; Fang and Zhang 2010), a wave pouch can protect a protovortex inside from strain/shear deformation and dry air intrusion above the boundary layer, and its cyclonic gyre also provides a focal point for vorticity aggregation. Wang et al. (2012) further examined the vertical structure of the wave pouches and suggested that a moist and convectively active wave pouch extending from the middle troposphere (600–700 hPa) down to the boundary layer is a necessary and highly favorable condition for TC formation. The marsupial paradigm provides a new perspective to look at the impacts of the large-scale circulation on TC formation.

In this study we will examine the variability of the Atlantic Hadley circulation and its impacts on TC activity. As discussed earlier, the Hadley circulation links various aspects of the large-scale circulation, and this study aims to provide a better understanding of the association between the large-scale circulation and TC activity. Using insights from the marsupial paradigm, we will also examine easterly waves as a “connecting link” between the large-scale circulation (its structure and variability) and TC development.

The remaining of the paper organizes as below. The data and methodology are described in Chapter 2. The interannual variability of the Atlantic Hadley circulation is presented and discussed in Chapter 3. The impacts of the interannual variability of the Atlantic Hadley circulation on TC activity are examined in Chapter 4, followed by a summary and discussion in Chapter 5.

CHAPTER 2: DATA AND METHODOLOGY

2.1 Data

Monthly mean wind data from NCEP–DOE Reanalysis 2 (NNR2; Kanamitsu et al., 2002) was used to derive the meridional streamfunction (defined in section 2.2) and examine the large-scale atmosphere circulation, and the 6-hour data from NNR2 were used to investigate the TEW activity. A 2.5 to 9-day band-pass filter and a 2.5-day low-pass filter were constructed (Doblas-Reyes and Déqué, 1998) and applied to the 6-hour wind data. The former was used to extract the TEWs, and the latter was used to remove the high-frequency fluctuations. The low-pass filtered data can be regarded as the "total" flow, which consists the mean flow and the wave perturbations. Besides NNR2, the ECMWF Interim Reanalysis (ERA-Interim) and the NCEP Climate Forecast System Reanalysis (CFSR) datasets were also used to examine the robustness of the findings. Since most features identified using NNR2 were found robust, the discussion is mainly focused on NNR2, and the comparison between different datasets is briefly addressed in Chapter 5. Monthly Sea Surface Temperature (SST) data from NOAA Extended Reconstructed Sea Surface Temperature v3b (ERSST; Xue et al., 2003; Simth et al., 2008) and monthly precipitation data from the Global Precipitation Climatology Project (GPCP; Adler et al., 2003) were also used in this study. Yin et al. (2004) suggested that GPCP represents the oceanic precipitation more reasonably than the CPC Merged Analysis of Precipitation (CMAP) does. The North Atlantic hurricane database (HURDAT, Landsea et al. 2008), which is also known as the best track data, was used to examine the TC activity, including genesis frequency, storm tracks and intensity. The index for the Atlantic equatorial mode (AEM) was derived from ERSST. Time series of several other climate indices were downloaded from the NOAA Physical Sciences

Division (PSD) (http://www.esrl.noaa.gov/psd/data/climateindices/list/) and were used to examine the linkage between different climate factors and the Atlantic Hadley circulation.

To investigate the links between the ITCZ and the Atlantic TC activity, we focus on the hurricane peak season, July-September (JAS) during 1979-2010. October was not included because the large-scale atmosphere circulation (including the Hadley circulation) in this month is quite different from the JAS mean. Consequently, the TC activity center shifts northwestward to the Caribbean Sea and the Gulf of Mexico, and more TCs develop with the subtropical origins while the role of TEWs diminishes.

2.2 Methodology

Stokes streamfunction has been commonly used to study the mean meridional circulation (e.g., Oort and Rasmusson, 1970; Oort and Yienger, 1996; Dima and Wallace, 2003). In this approach, the meridional circulation was assumed to be non-divergent, i.e., $\frac{\partial v}{\partial y}+\frac{\partial \omega}{\partial p}=0$, or there is no net mass flux in the zonal direction. A streamfucntion can thus be defined for the meridional circulation, which satisfies (Oort and Yienger, 1996):

$$[\bar{v}]=g\frac{\partial \psi}{2\pi R\cos\phi \partial p} \quad (1)$$

$$[\bar{\omega}]=-g\frac{\partial \psi}{2\pi R^2\cos\phi \partial \phi} \quad (2)$$

where v is the meridional velocity, ω is the vertical velocity in pressure coordinates, ψ is Stokes streamfunction, R is the mean radius of the earth, ϕ is latitude, and the overbar and the brackets denote temporal and zonal averaging, respectively. Stokes streamfunction is often derived by vertical integration of the meridional wind based on Eq. (2):

$$\psi = \frac{2\pi R}{g}\int [\bar{v}]\cos\phi dp \qquad (3)$$

The assumption of non-divergent meridional circulation is valid over the global domain, but it breaks down over regional domains or individual basins when the zonal mass transport in or out of the domain is not negligible. To study the variability of the Atlantic Hadley circulation, we took an original approach to define the streamfunction. Recall that the horizontal wind field can be decomposed into the nondivergent and irrotational components, and only the irrotational component contributes to the vertical motion. The irrotational component of the meridional flow can be regarded as part of the north-south overturning circulation, i.e., the Hadley circulation, and the irrotational component of the zonal flow can be regarded as part of the east-west overturning circulation, i.e., the Walker circulation. We can thus divide the vertical velocity into two parts, one associated with the Hadley circulation, and one with the Walker circulation:

$$\frac{\partial v_\chi}{\partial y} + \frac{\partial \omega_H}{\partial p} = 0 \qquad (4)$$

$$\frac{\partial u_\chi}{\partial x} + \frac{\partial \omega_W}{\partial p} = 0 \qquad (5)$$

where the subscript χ denotes the irrotational wind component; the subscripts H and W denote the Hadley circulation and the Walker circulation, respectively; the sum of ω_H and ω_W yields the total vertical motion. Note that such partitioning does not imply that the zonal and the meridional circulations are independent of each other. The coupling of zonal and meridional circulations has been suggested responsible for the inter-basin association (e.g., Chang et al. 2000; Chiang et al. 2002).

Using Eq. (4), the meridional streamfunction for the Hadley circulation can be derived based on the irrotational component of the meridional flow:

$$\psi = \frac{2\pi R}{g}\int [v_\chi]\cos\phi dp \qquad (6)$$

where downward integration was applied by assuming ψ=0 at the top of the atmosphere. To study the interannual variability of the Hadley circulation over the Atlantic, the JAS seasonal mean meridional wind was averaged over 20°W-70°W to derive the streamfunction. The Empirical Orthogonal Function (EOF) and composite analyses were then used to extract the dominant modes of the interannual variability and examine their impacts on TCs.

CHAPTER 3: MERIDIONAL STREAMFUNCTION ANALYSIS

The JAS mean meridional streamfunction over the Atlantic averaged over 1979-2010 is shown in Fig. 1a. Between 60°S and 60°N, there are four circulation cells. The most prominent cell is the southern Hadley Cell, with the upward motion slightly north of the equator and the downward motion around 15°S. The amplitude of the streamfunction associated with this cell is about -2.2×10^{11} kg s^{-1}, which is comparable to the global average reported in previous studies (e.g., Oort and Yienger 1996; Dima and Wallace 2003; Mitas and Clement 2005; Stachnik and Schumacher 2011). The northern Hadley Cell is much weaker in amplitude and has a shallower vertical structure. The asymmetry of the Hadley circulation between the winter and the summer hemispheres has been discussed in previous studies (e.g., Lindzen and Hou 1988). Farther poleward of the Hadley Cells are the so-called Ferrel Cells, with subsidence in the subtropics and ascent at the higher latitudes. Figure 1b shows the standard deviation of the interannual variability. The strong variations occur in the tropical troposphere, collocating with the southern Hadley Cell. The linear trend during the 32-year period is shown in Fig. 1c.The southern Hadley Cell is strengthened at the pace of $0\sim3\times10^{10}$ kg s^{-1} per decade and its northern boundary extended northward. The southern Ferrel Cell is also strengthened but with a much weaker trend.

The EOF analysis was applied to the streamfunction field between 60°S to 60°N, from 1000 hPa to 100 hPa to extract the dominant modes of the interannual variability. To ensure the physical robustness of the EOF analysis (Lian and Chen 2012), the linear trend was removed from the streamfunction field at every grid point before applying the EOF analysis. As shown in Fig. 2a, the strong variability in the tropics is well captured by the first EOF mode (hereafter M1), which is similar to the asymmetric mode, or the so-called ‘‘solsticial pattern” (Dima and

Wallace 2003). M1 is mainly related to the variability of the southern Hadley Cell, with a strong cell centered slightly south of the equator; a weaker cell of opposite sign is centered near 30°N, far north from climatology center of the northern Hadley Cell. This dipole pattern and the associated strong zonal gradient of streamfunction at 0-10°N imply that M1 is closely associated with variations of the ITCZ vertical motion. Since M1 explains nearly half (46%) of the total variance, this dominant mode will be the focus in this paper.

To better illustrate the variability of the Hadley circulation associated with M1, we constructed the streamfunction composites using six strongest positive years (1979, 1988, 1995, 1996, 1999, 2010) and the six strongest negative years (1983, 1986, 1994, 1997, 2002, 2009) according to the time series of M1. Fig. 2c and 2d show that the positive (negative) phase of M1 is featured by a stronger (weaker) and more (less) extensive southern Hadley Cell and the upward motion is enhanced (reduced) and becomes more (less) extensive in the ITCZ. The northern Hadley Cell remains weak in both composites, but a close look indicates that the streamfunction gradient, and thus the subsidence, is reduced in the subtropics between 20°N-30°N during the positive phase. Figure 2 suggests that the variability of the ITCZ, although located north of the equator, is mainly related to the variations of the southern Hadley Cell.

The composite difference of precipitation between the positive and negative phases of M1 is shown in Fig. 3. A basin-wide precipitation increase occurs over the Atlantic between 0-30°N in the positive phase. In particular, precipitation is enhanced significantly along 7°N over Guiana Highlands, the East Atlantic ITCZ, and between 15°N-20°N over the West Atlantic and the Caribbean Sea. The former two changes confirm that M1 is associated with the intensity change, rather than meridional displacement, of the ITCZ; and the latter is likely associated with the enhanced TEW and TC activity. Precipitation also increases over Central America and

northern South America. In contrast, the precipitation in the Eastern Pacific ITCZ is greatly reduced, which is related to the ENSO pattern over the Pacific as discussed later in this chapter.

To investigate what may cause the intensity change of the ITCZ, we calculated the correlation between M1 and some prominent climate factors. For the consistency with the EOF analysis, all the JAS mean time series were first detrended. As shown in Table 1, M1 is significantly correlated (above 99% confidence level) with Niño 3.4, the AMM, the Atlantic Equatorial Mode (AEM, represented by averaged SST in 0-20°W, 4°S-4°N), the Atlantic hurricane number (during JAS) and the Sahel precipitation index (Standardized gauge precipitation averaged over 8°N-20°N, 20°W-10°E). The simultaneous correlation between M1 and the Atlantic Multidecadal Oscillation (AMO) is relatively weak and below 95% confidence level, and the linear correlation in the case of M1 and North Atlantic Oscillation (NAO) is nearly zero.

The composite difference of SST based on M1 (Fig. 4) reveals a mixed pattern. The most prominent signature is the SST cooling over the East and Central Pacific, or the La Niña-like pattern. Although ENSO peaks in boreal winter, the magnitude of the SST difference over the East Pacific is up to 1.8 K. It is interesting to notice that the basin-wide SST pattern at the Atlantic resembles that at the Pacific but with the opposite polarity: positive values are found at the tropical Atlantic while the negative values appear at the subtropical western parts. The SST signature over the western Tropical North Atlantic (TNA) is related the locally reduced trade wind. A similar process is also seen in the springtime development of AMM mode (e.g., Vimont et al. 2007), but mainly at the eastern TNA. Significant SST warming is also centered near (40°N, 20°W). At equatorial Atlantic, the off-shore SST signature over the equatorial East

Atlantic projects on the AEM mode. Note that the meridional SST gradient is enhanced near the south of the equator but weakened on its north edge due to the equatorial warming.

One direct impact of La Niña-like pattern is the weakened East Pacific ITCZ, which contributes to an anomalous Walker circulation. The associated low-level westerly anomalies and upper-level easterly anomalies between 130°W-30°W reduce the vertical shear of zonal wind over Atlantic (figure not shown). Meanwhile, the low-level trade wind is weakened over the Caribbean Sea and the western NTA, which contributes to increased local SST via air-sea interactions (e.g., wind-evaporation-SST feedback). The AEM warming is associated with the reduced trade wind at the western equatorial Atlantic through the Bjerknes feedback mechanism (Keenlyside and Latif 2007). Lübbecke et al. (2010) suggested that the variations of trade wind are related to the variability of south Atlantic anticyclone, which is consistent with the analysis results (Fig. 2).

The lag correlations of 3-month mean time series are shown in Table 2. The lag correlation between Niño 3.4 and M1 exceeds the 99%-confidence level when Niño 3.4 leads M1 by 3 months (in the April-May-June mean), and the coefficient is strongest (-0.66) when Niño 3.4 leads M1 by 1 month. The lag correlation of AMM with M1 is above the 95% confidence level from FMA (AMM leads M1 by 5 months) to JJA, and the coefficient increases with decreasing lead time. Interestingly, a significant correlation (-0.47) between M1 and NAO briefly appeared in the preceding spring. The associated near-surface wind anomalies seem coupled with the dipole-like SST anomalies at the mid-latitude North Atlantic which contribute to the aforementioned extratropical SST signature (figure not shown). These lag correlations suggest that M1 may be forced by multiple climate modes and has the potential of predictability on the seasonal time scale.

In summary, the dominant mode of the interannual variability of the Hadley circulation is associated with the intensity variations of the ITCZ and is correlated to multiple climate factors. Some of these factors are not independent of each other. For example, the AMM mode may be excited by ENSO (e.g., Enfield and Mayer 1997); the extratropical forcing, such as NAO, may induce SST anomalies in the tropical Atlantic (Chiang et al. 2004; Sutton and Hodson 2007; Smirnov and Vimont 2012); and tropical SST anomalies may in turn lead to extratropical SST anomalies (Czaja and Frankignoul, 2002). The analysis implies a scenario in which the collaboration of these factors leads to M1, a prominent mode of the Hadley circulation over Atlantic. Some of the factors, such as ENSO and AMM, have been known to impact the Atlantic TC activity. In the next chapter, we will examine the impacts of M1 on the Atlantic TC activity.

CHAPTER 4: IMPACTS OF THE VARIABILITY OF THE HADLEY CIRCULATION ON THE ATLANTIC TCS

To examine the impacts of M1 on the Atlantic TC activity, we constructed the storm track composites for the positive and negative phases of M1 (Fig. 5). The colors along the tracks indicate the storm intensity. The most striking difference is that a larger number of TCs developed in the positive phase composite: there are 59 storms in the six positive-phase composite years and 34 storms in the six negative-phase composite years, while the average storm number in JAS during 1979-2010 is about 8.3. Comparison of the composites reveals a substantial increase in the number of TCs forming over the MDR in the positive phase. Developing over the open ocean, these storms have a longer time traveling over the warm ocean and thus a larger chance to develop into a major hurricane (Vimont et al. 2007; Kossin et al. 2007). Among the 59 TCs, there are 35 (~59%) hurricanes and 22 (~37%) major hurricanes (category 3 or above). In the negative phase of M1, TC genesis shifts northwestward, and there is a larger fraction of TCs forming near the southeast coast of the United States. These storms had short tracks before landfalling or curving northward. Even some of the MDR storms also had very short tracks, and only two MDR TCs tracked across the Caribbean Sea, leaving the ocean south of the Greater Antilles free from TCs. Among the 34 storms, there are only 15 (~44%) hurricanes and 6 (~18%) major hurricanes, which is in sharp contrast to the positive phase composite.

The composites of M1 suggest that the variations of the Atlantic TC activity (JAS) are closely related to the variations of the Hadley circulation, or more specifically, the ITCZ intensity changes. The composites of other leading EOF modes did not reveal any associated TC

variability very clearly, which is consistent with their limited contribution to the interannual variability of the Atlantic Hadley circulation. In the following we will investigate how M1 affects the Atlantic TC activity.

4.1 The Large-scale Environment

Fig.4 shows that the MDR SST in the positive phase is about 0.5 K warmer than that in the negative phase. The warmer SST favors TC formation and intensification, but the changes of the large-scale conditions induced by SST anomalies are likely more important than the direct thermodynamic impacts of warmer local SST (Swanson 2008). As mentioned in the previous chapter, the low-level westerly anomalies and the upper-level easterly anomalies associated with an anomalous Walker circulation reduce the VWS over the most part of the MDR, the Gulf of Mexico, and especially over the Caribbean Sea, where the VWS difference between the positive and negative phases is as large as 8 m s^{-1} (Fig. 6a). Differences of VWS with a similar pattern and a smaller magnitude are also found in the lower troposphere (between 500 and 850 hPa, Fig. 6b). Strong VWS has long been known detrimental for TC formation and intensification (e.g., Gray 1968; DeMaria et al. 1996), and reduced (enhanced) VWS in the positive (negative) phase of M1 contributes to a more (less) active hurricane season over the Atlantic.

The composite difference of the isobaric vertical velocity between the positive and negative phases of M1 is shown in Fig. 7a. Upward velocity anomalies are found between 6°S and 26°N with two maxima. The maximum ascent enhancement between 5°S and 5°N is consistent with the changes in the streamfunction field (Fig. 2c, d) and indicates a stronger and meridionally more extensive upward branch of the southern Hadley Cell. What is more directly

relevant to TC activity is the upward velocity anomalies between 10°N-20°N throughout the troposphere, which is related to a northward extended ITCZ or reduced subsidence to its north.

Fig. 7b shows the composite anomalies of relative humidity (RH) based on M1. Strong positive RH anomalies are found over the equatorial zone throughout the troposphere, and weaker, but significant positive RH anomalies also appear between 10°N-30°N. The former is related to the stronger and more extensive ITCZ, and the latter is likely due to the weakened subsidence associated with the northern Hadley cell. Correspondingly, the Convective Available Potential Energy (CAPE) (from the ERA-Interim reanalysis) increases along the northern wave track over Africa and in the ITCZ and MDR regions east of 70°W while decreasing over the Caribbean Sea and the Gulf of Mexico (Fig. 8). Middle-level moisture has long been recognized as a necessary condition for TC formation (e.g., Gray 1968). The recent study by Fritz and Wang (2012) suggested that the persistent upper-level dry air was also detrimental for TC formation. A moist column throughout the troposphere is thus favorable for TC formation and contributes to the increase of TC frequency in the positive phase of M1.

The subtropical subsidence is closely related to the subtropical high. The weakened subsidence over the subtropical North Atlantic implies a weaker subtropical high in the positive phase of M1, which is confirmed by the composites of 500 hPa geopotential height. As shown in Fig. 9, the subtropical high in the positive phase is weaker and retreats eastward compared to the negative phase. The impacts of the subtropical high on Atlantic tropical storm tracks have been noted by numerous studies (e.g., Kossin et al., 2010; Colbert and Soden, 2012). The associated steering flow allows TCs to curve northeastward over the East and Central Atlantic (Fig. 5). Meanwhile, the decrease of CAPE storage also makes the Caribbean Sea less favorable for TC

activity. Consequently, the number of landfalling storms does not increase proportionally with the total TC number (Fig. 5).

We also examined the changes of the low-level and middle-level divergence and vorticity associated with M1 (figure not shown). During the positive phase, the positive vorticity anomalies and enhanced convergence were found in the lower troposphere over the MDR. The convergence in the planet boundary layer (PBL) intensified over the MDR, especially over the West Atlantic. The enhanced PBL convergence favors TC activity by pumping more moisture upward and increasing the humidity in the free atmosphere. The increase in cyclonic vorticity, most pronounced at 600 hPa and 700 hPa levels, extends from West Africa and also largely overlaps MDR.

In summary, various aspects of the large-scale conditions are favorable for TC formation and intensification in the positive phase of M1. This, however, is not the complete story. One of the necessary conditions for TC formation in the present climate is a pre-existing low-level cyclonic disturbance. The TC genesis location affects the subsequent development of a storm as discussed earlier in this chapter. In the next section we will examine the hypothesis that the variability of the Hadley circulation can impact the Atlantic TC activity indirectly via modulating the frequency and structure of TEWs.

4.2 Tropical Easterly Waves

To examine the variations of the TEW activity, we calculated the eddy kinetic energy (EKE) of the 2.5 to 9-day band-pass filtered 850 hPa wind and constructed the composites based on the positive and negative phases of M1. Figure 10a shows the positive composite. A strong wave center was found at the west coast of Africa around 12°N, where AEWs usually get

intensified through interaction with mesoscale convective systems (Berry et al. 2005; Ventrice et al. 2012). The wave activity can be tracked east of the Prime Meridian, and a second track along 20°N is also discernible, which is related to eastward propagating disturbances north of the African easterly jet (Pytharoulis and Thorncroft 1999). The wave activity extends westward to the ocean but weakens away from the coast. The strong variances over the subtropical western North Atlantic can be attributed to TEWs, midlatitude disturbances and TCs.

Figures 10b and 10c show the composite of the wave activity in the negative phase and the composite difference between the positive and negative phases, respectively. Compared to the positive phase, the wave activity is reduced over West Africa, along the wave track over the MDR, the Caribbean Sea and the Gulf of Mexico. Enhanced wave activity in the positive phase of M1 was also found at 700 hPa, especially near the West Africa coast. Large variances can be attributed to strong waves and/or more frequent occurrence of waves. The increases in wave strength (e.g., Arnault and Roux 2011) and frequency (e.g., Thorncroft and Hodges 2001) both have been noted as favorable for TC activity.

AEWs can be regarded as perturbations excited by finite-amplitude, transient heating in a linearly stable mean state (Thorncroft et al. 2008). The mean flow may not be unstable enough to maintain or amplify the waves, but the idealized simulation by Leroux et al. (2009) showed that the wave response is very sensitive to the structure of the mean flow. Strong waves are associated with a strong jet that has a strong vertical shear in the lower troposphere or a strong and extended potential vorticity reversal. The composites of the 700 hPa seasonal mean (JAS) zonal flow are shown in Fig. 11. Over West Africa and the East Atlantic, although the easterly jet has a similar intensity in the positive and negative composites, the jet in the positive composite is characterized by a stronger cyclonic shear south of the jet core and a larger area of absolute

vorticity gradient reversal. The enhanced cyclonic shear is mainly contributed by the weaker easterly flow south of 12°N. The extended area of absolute vorticity gradient reversal implies the stronger instability and thus a better chance for wave growth. The composites of 850 hPa zonal wind show that the low-level westerly flow is also enhanced (not shown). The stronger monsoonal westerly increases moisture convergence near the coast and favors coastal development of AEWs. Meanwhile, the enhanced upstream AEW activity, which is consistent with the CAPE increase (Fig. 8), also favors the coastal development. The variations of the TEW activity can be thus attributed to the change of the mean flow and the change of convective activity near the coast of West Africa.

Besides the wave frequency and intensity (Thorncroft and Hodges 2001; Camara et al. 2011), another aspect of the TEWs that affects their subsequent evolution is the wave structure, in particular, the existence and structure of the wave pouch (Wang et al. 2012; Hopsch et al. 2010). Next we will examine the wave pouch frequency and vertical coherence for the positive and negative phases of M1.

A wave pouch is a region of cyclonic rotation and weak deformation. We use the following two criteria to estimate the wave pouch frequency: i) $OW>1.0\times10^{-10}$ s^{-2} and ii) $\zeta>1.0\times10^{-6}$ s^{-1}, where ζ is the relative vorticity, and the Okubo-Weiss (OW) parameter is defined as the square of vorticity minus the squares of the normal and shear components of flow strain (Rozoff et al. 2006). The positive values of OW indicate that the flow is rotation-dominant. Instead of the 2.5 to 9-day band-pass filtered data, the 2.5-day low-pass filtered data were used to calculate the pouch frequency as the background flow needs to be taken into account for the formation of a wave pouch. Also note that the threshold of OW used here is relatively small. This is to take into account the filtering of high-frequency fluctuations and to include weak wave

pouches that did not develop into TCs. To exclude the impacts of TCs, all the grid points within a 12.5 degree circle centered on a TC along 6-hourly HURDAT TC tracks were not counted.

The composite of 850 hPa wave pouch frequency in the positive phase of M1 is shown in Fig. 12a. The non-zero pouch frequency region follows the wave track, which is south of the jet over North Africa and extends westward and slightly northward all the way to the southeast coast of the United States. High frequency of occurrence is found along the northern and southern wave tracks over West Africa and along the wave track over the East Atlantic, with a maximum off the coast of West Africa. The center of high frequency near Panama is caused by shallow stationary vortices that are typically irrelevant with Atlantic TC activity. Cyclogenesis locations, especially for the MDR storms, largely fall into the regions of high pouch frequency. The composite of the pouch frequency for the negative phase of M1 and the differences between the positive and negative phase composites are shown in Figs. 12b and 12c, respectively. Significant reduction of the pouch frequency is found along the wave track over West Africa, the Atlantic MDR and the Caribbean Sea, which is consistent with the reduced TC activity.

To examine the vertical structure of wave pouches, we examine the frequency of occurrence of "deep" wave pouches in the lower troposphere. The vorticity and OW were examined at 500, 600, 700, and 850hPa levels over each grid point, and a wave pouch is designated as a deep pouch if at least 3 out of 4 levels satisfy the abovementioned criteria. This is to exclude shallow or strongly tilted wave pouches. The procedure to exclude the TC circulations remains the same. As shown in Fig. 13a, high frequency of deep pouches of 10-14 days per season occurs along 10°N-12°N over West Africa and the East Atlantic in the positive phase of M1. The northern wave track over West Africa is still discernible but has a much lower frequency than the southern one. This is consistent with previous findings that the northern

waves generally have a shallow structure confined to 850 hPa and below (e.g., Pytharoulis and Thorncroft 1999). The composite based on the negative phase of M1 (Fig. 13b) has a similar spatial pattern, but the frequency of deep pouches is significantly reduced along the wave track over West Africa and the East Atlantic, over the Caribbean Sea, and over Central America.

The above diagnoses suggested that the ITCZ affects the Atlantic TC activity indirectly via modulating the wave pouch frequency and structure and that in the positive phase of M1 waves tend to develop a more favorable pouch structure for TC formation. It should be pointed out that the variations of the TEWs are not independent of the variations of the large-scale circulation. For example, the warm SST, upward velocity anomalies and a moist troposphere associated with the stronger ITCZ (the positive phase of M1) and the anomalous Walker Circulation are conductive to convective development, which is believed to play an important role in the maintenance and intensification of TEWs (e.g., Berry et al. 2005; Thorncroft et al. 2008). Interaction between a TEW and the ITCZ can also produce a stronger and deep wave pouch (Wang et al. 2012). A wave pouch is more likely to develop a vertically coherent structure if the VWS is weak (Wang et al. 2012; Raymond et al. 2011; Davis and Ahijevich 2012).

CHAPTER 5: SUMMARY AND DISCUSSION

The interannual variability of the Hadley circulation in boreal summer and its impacts on the Atlantic TC activity were examined in this study. An original method was developed to define the regional Hadley circulation in terms of the meridional streamfunction that is derived from the irrotational component of the meridional flow. The long-term mean summer seasonal streamfunction over the Atlantic consists of a prominent southern Hadley Cell and a dwarfed northern Hadley Cell, which is similar to the solistical pattern in the global streamfunction average (Lindzen and Hou 1988; Dima and Wallace 2003).

The EOF analysis was employed to study the interannual variability of the Hadley circulation over the Atlantic. The leading mode explains more than 45% of the total variances and is mainly associated with the variations of the southern Hadley Cell and the intensity change of the ITCZ. It was found that M1 is significantly correlated to multiple climate factors, including ENSO, AMM, NAO, and the Sahel precipitation and that the Atlantic TC activity is strongly impacted by M1. In the positive phase of M1 (when the ITCZ is stronger than normal), there are more TCs forming over the MDR with a larger fraction intensifying into major hurricanes. In the negative phase of M1, the Atlantic TC genesis frequency is lower than normal, and the genesis locations shift northwestward to the Gulf of Mexico and the western North Atlantic. Composite analyses showed that the positive phase of M1 is characterized by warmer SST, weaker VWS, higher water vapor content throughout the troposphere, larger CAPE, the enhanced low-level convergence, as well the stronger middle-level vorticity over the MDR, all of which are favorable for the TC formation and intensification.

The role of TEWs in modulating the Atlantic TC activity is highlighted in this study. In the positive phase of M1, the wave activity (in terms of EKE of band-pass filtered data) is significantly enhanced over the East Atlantic and the Caribbean Sea, which can be attributed to stronger coastal convection and a more unstable mean flow with extended area of the absolute vorticity gradient reversal. In the context of the recently proposed marsupial paradigm (Dunkerton et al. 2009), we also examined the frequency and structure of the wave pouches associated with different phases of M1. In the positive phase of M1, wave pouches occur more frequently at 850 hPa over the MDR, and the number of wave pouches with a vertically coherent structure also increases significantly. The vertically coherent structure of the wave has been suggested a necessary and highly favorable condition for the TC formation (Wang et al. 2012). This study thus suggests that the variability of the Hadley circulation impacts the Atlantic TC activity by modulating the large-scale conditions as well as the frequency and structure of TEWs. The perspective based on the Hadley circulation thus provides a more complete dynamic framework to understand the cooperative impacts of the different aspects of the large-scale circulation on the TC activity.

This diagnosis showed that M1 and the AMM are significantly correlated with each other. The AMM is a dominant mode of air-sea interaction over the Atlantic, and also has strong impacts on the Atlantic TCs (Xie et al. 2005; Vimont and Kossin 2007; Kossin and Vimont 2007). However, M1 is not simply a manifestation of the atmospheric component of the AMM mode. First, M1 mainly represents the intensity variability of ITCZ, while AMM is featured by the meridional displacement of ITCZ during Aug-Oct (Smirnov and Vimont 2011). Second, other climate factors, such as ENSO and NAO, are also significantly correlated with M1. This suggests that these climate factors affect the Atlantic TCs by modulating the Hadley circulation.

The diagnoses presented in this study are mainly based on the NNR2 data. To check the robustness of the results, similar analyses were done using the ERA-Interim data and the CFSR reanalysis data. An intensifying and expanding trend of the southern Hadley Cell was found in all datasets, albeit with quantitative differences in the spatial pattern and in the intensification rate. Although the higher order EOF modes are sensitive to the datasets, the leading mode was found quite robust. The leading EOF modes in different datasets share the similar dipole pattern, representing the intensity variations of the ITCZ, and the spatial correlation coefficients between M1 in different datasets range from 0.89 to 0.94. The variances explained by the leading mode vary between 45% and 56%. We also tested the robustness of the EOF analysis by varying the longitude range over which the streamfunction was averaged, and M1 remains robust when the zonal domain is reduced from 20°W-70°W to 20°W-50°W. These tests thus suggest that M1, i.e., the intensity variability of the ITCZ, is the dominant mode of the interannual variations of the Atlantic Hadley circulation during boreal summer.

FIGURES AND TABLES

Table 1. Correlation between M1 and detrended climate indices (JAS). Correlations in italic bold are above the 99% significance level and the rest are below the 95% significance level.

	Hurr. num	Niño 3.4	AMM	AMO	AEM	Sahel	NAO
M1	***0.66***	***-0.65***	***0.53***	0.34	***0.47***	***0.52***	-0.02

Table 2. Lag correlation between M1 (JAS) and detrended climate indices. Correlations in italic and brackets are above the 95%-confidence level, and correlations in italic bold exceed the 99%-confidence level.

	JFM	FMA	MAM	AMJ	MJJ	JJA	JAS
Niño 3.4	-0.01	-0.08	-0.24	***-0.46***	***-0.62***	***-0.66***	***-0.65***
AMM	0.34	*(0.36)*	*(0.39)*	***0.45***	***0.49***	***0.49***	***0.53***
NAO	-0.25	*(-0.37)*	***-0.47***	-0.27	-0.11	0.05	-0.02

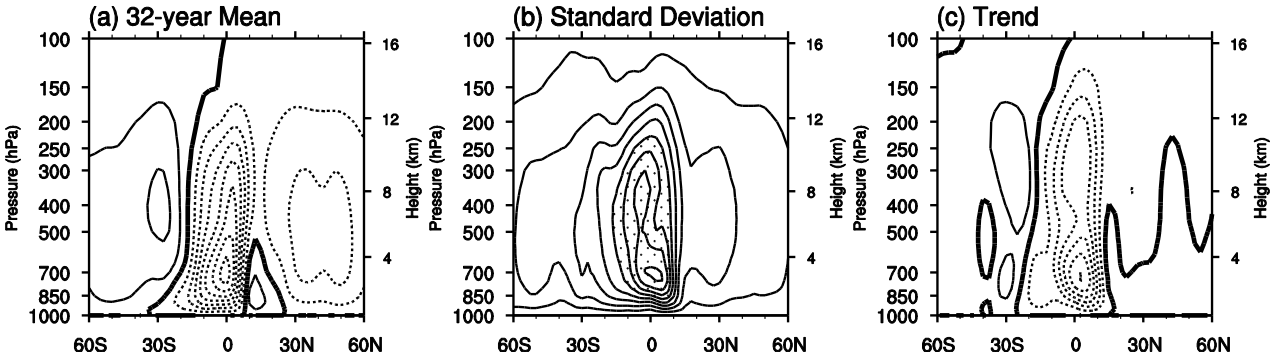

Figure 1. (a) 32-year mean (10^{11} kg s^{-1}), (b) standard deviation (10^{10} kg s^{-1}), and (c) 32-year trend (10^{9} kg s^{-1} yr^{-1}) of the JAS seasonal mean streamfunction. Zero lines are thickened in (a) and (c), and solid (dash) lines indicate positive (negative) values. Contour intervals are (a) 0.3×10^{11} kg s^{-1}, (b) 0.5×10^{10} kg s^{-1}, (c) 0.5×10^{9} kg s^{-1} yr^{-1}, respectively. Values greater than 2.5×10^{10} kg s^{-1} are shaded in (b).

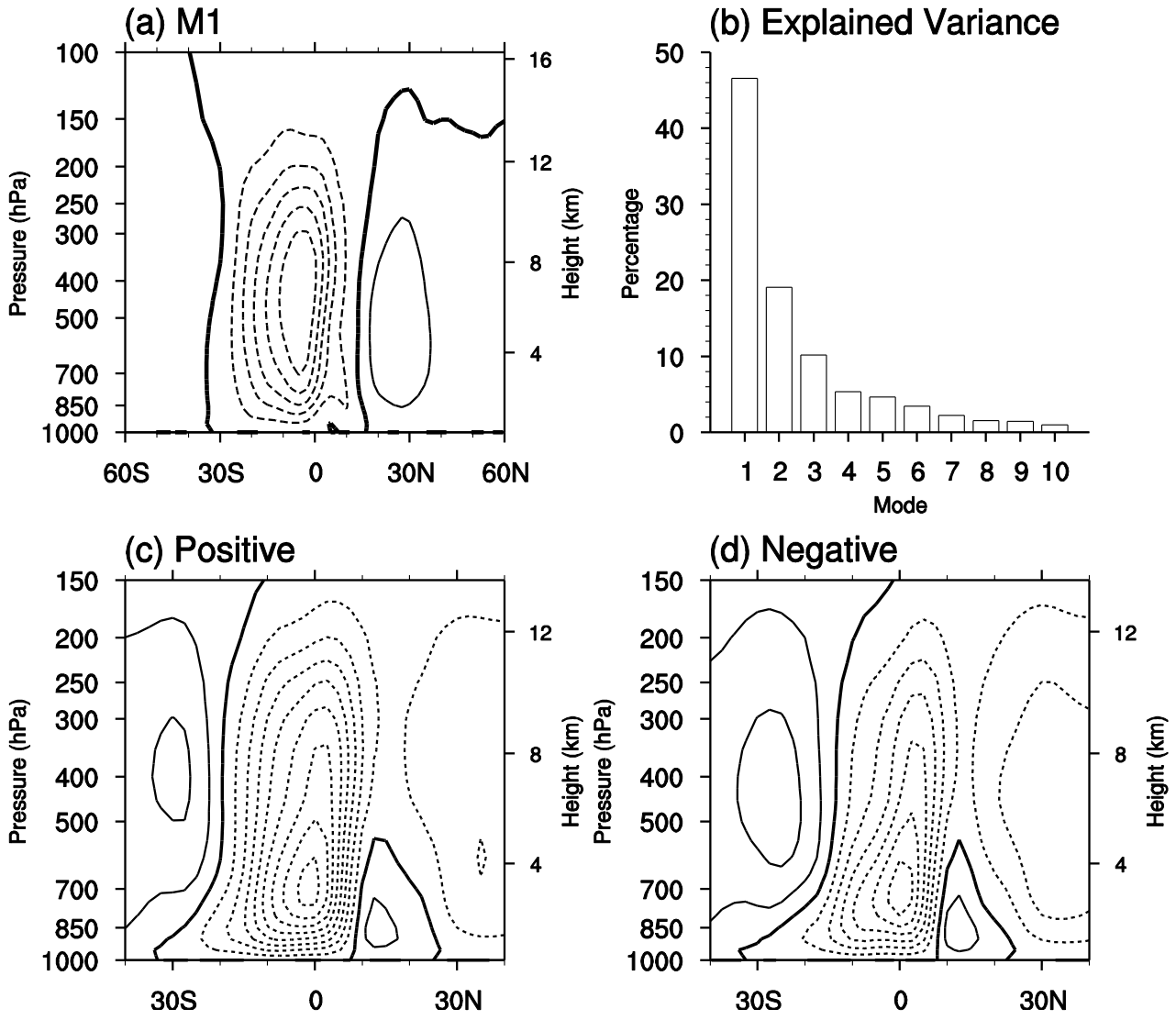

Figure 2. EOF analysis of Meridional Circulation (JAS). (a) The leading mode (M1), (b) variance explained by the first 10 modes, streamfunction composites (10^{11} kg s^{-1}) for the (c) positive and (d) negative phases of M1. Zero lines are thickened in (a) (c) and (d), and solid (dash) lines indicate positive (negative) values. Contour intervals are (a) 0.02 and (c) (d) 0.3×10^{11} kg s^{-1}, respectively.

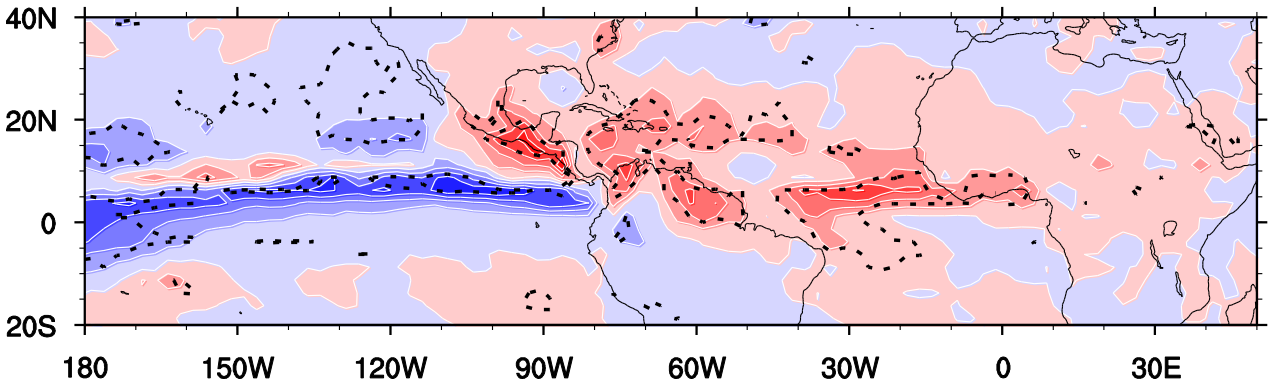

Figure 3. Composite difference of precipitation based on M1 (units: mm day^{-1}). Dashed black line indicates the precipitation differences passing the Student-t 95% confidence test.

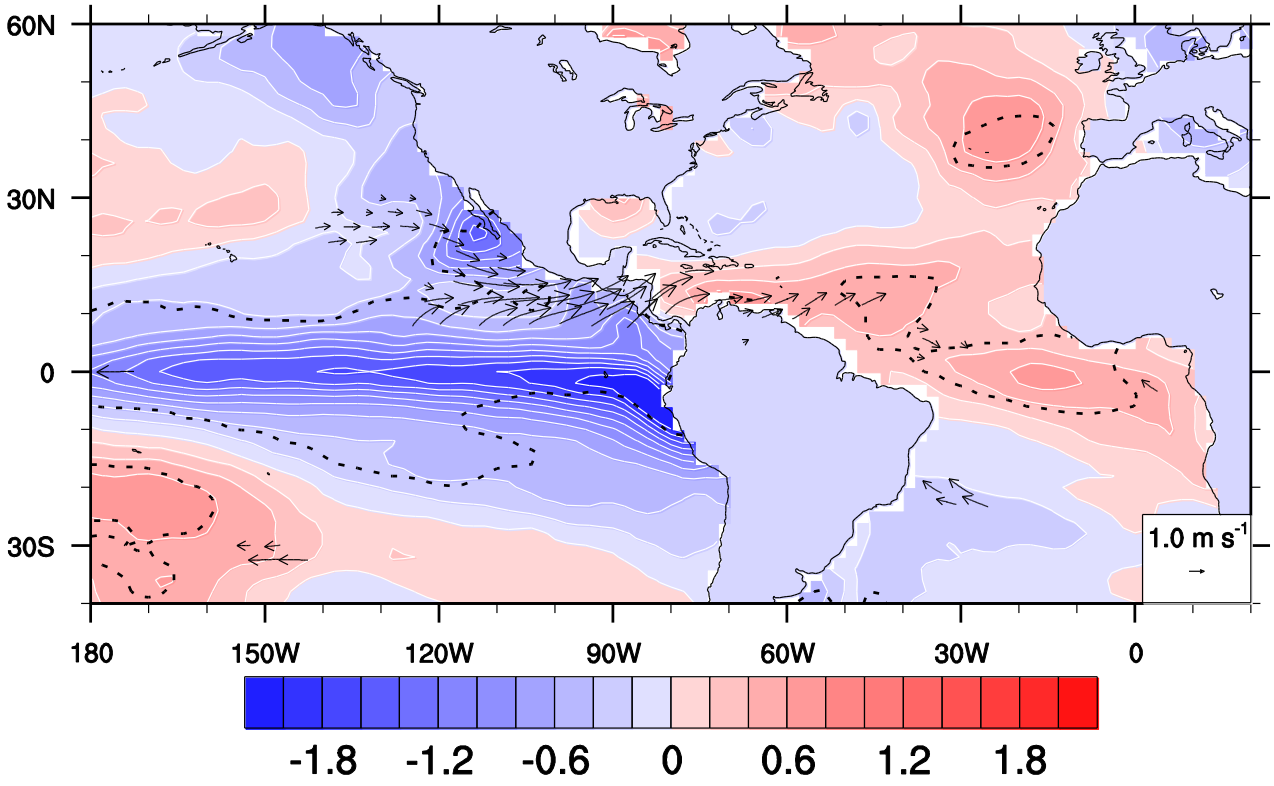

Figure 4. Composite difference of SST (color) and 10-m wind vector based on M1. Dashed black line indicates the SST signal passes Student-t 95% confidence test. Only 95%-confidence part of wind vectors is plotted.

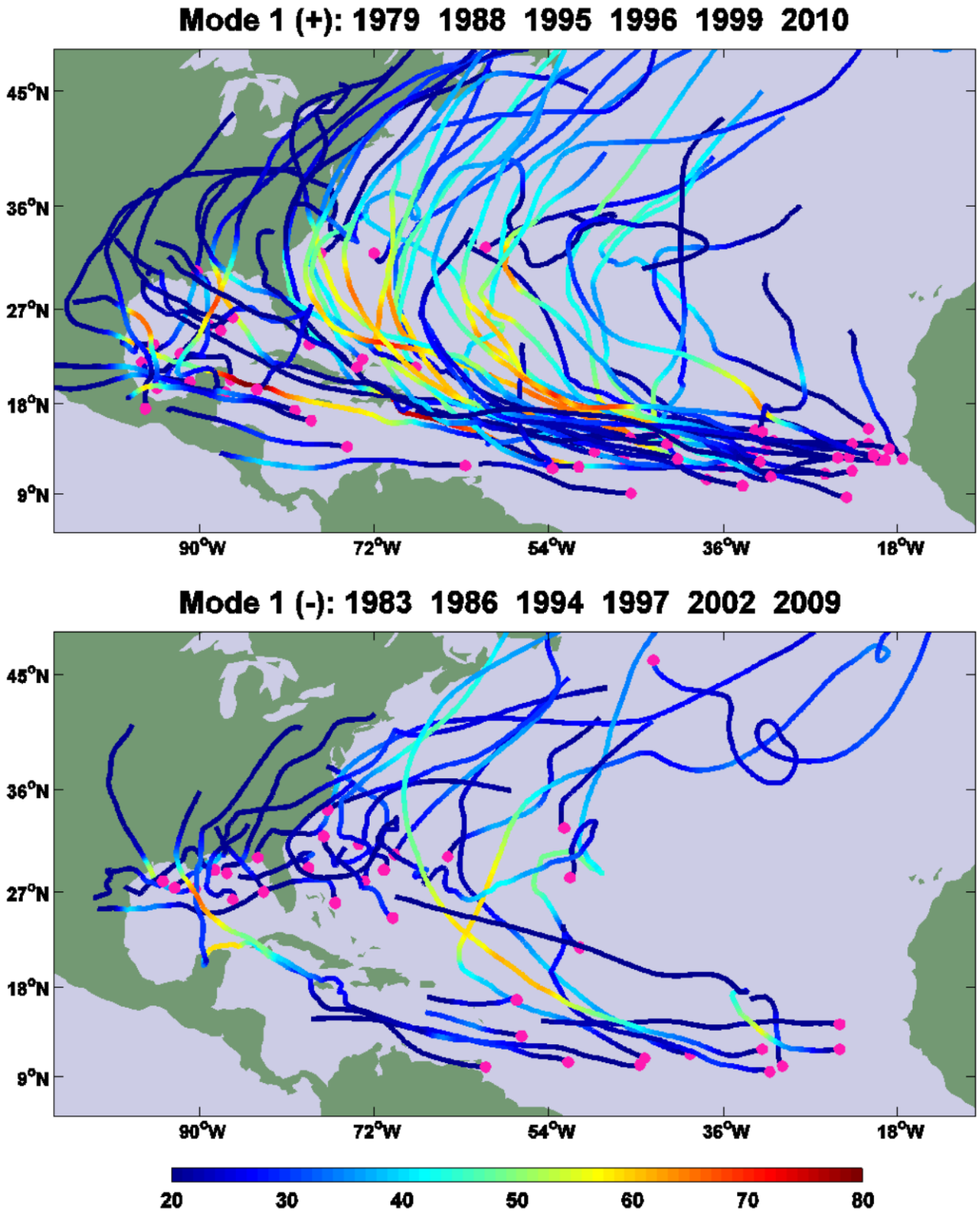

Figure 5. Storm track, intensity and genesis location (JAS) for the positive and negative phases of M1. Genesis locations are indicated by the pink dots, and the storm intensity in terms of the maximum surface wind speed (m s^{-1}) is indicated by colors of storm tracks. The composite years for each phase are listed at the top of each plot.

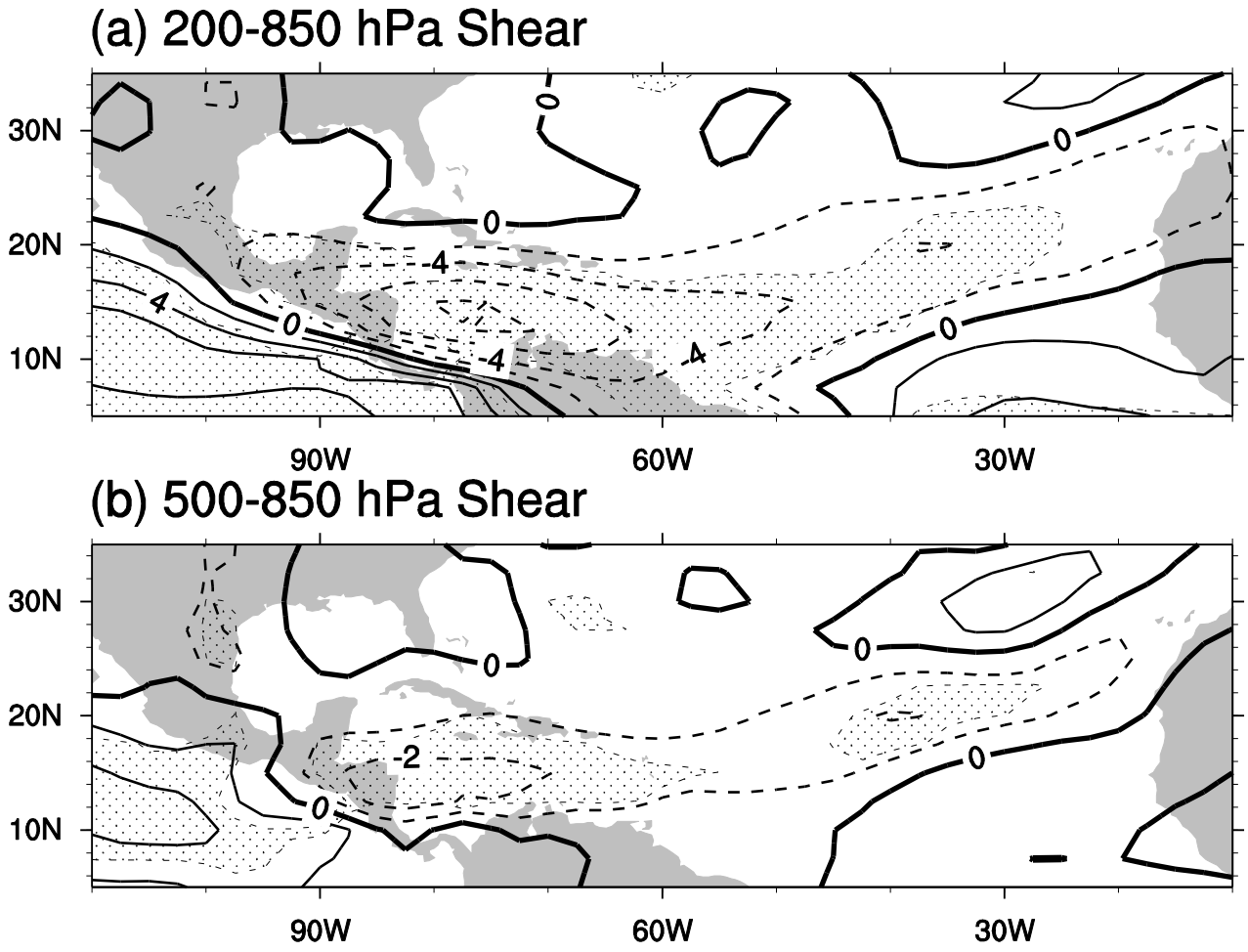

Figure 6. Composite differences of (a) the 200-850 hPa and (b) the 500-850 hPa vertical wind shear (vector wind difference). Contour intervals are (a) 2.0 m s^{-1} and (b) 1.0 m s^{-1}, respectively. Zero lines are thickened, and solid (dash) lines indicate positive (negative) values. Shading indicates differences above the 95% confidence test.

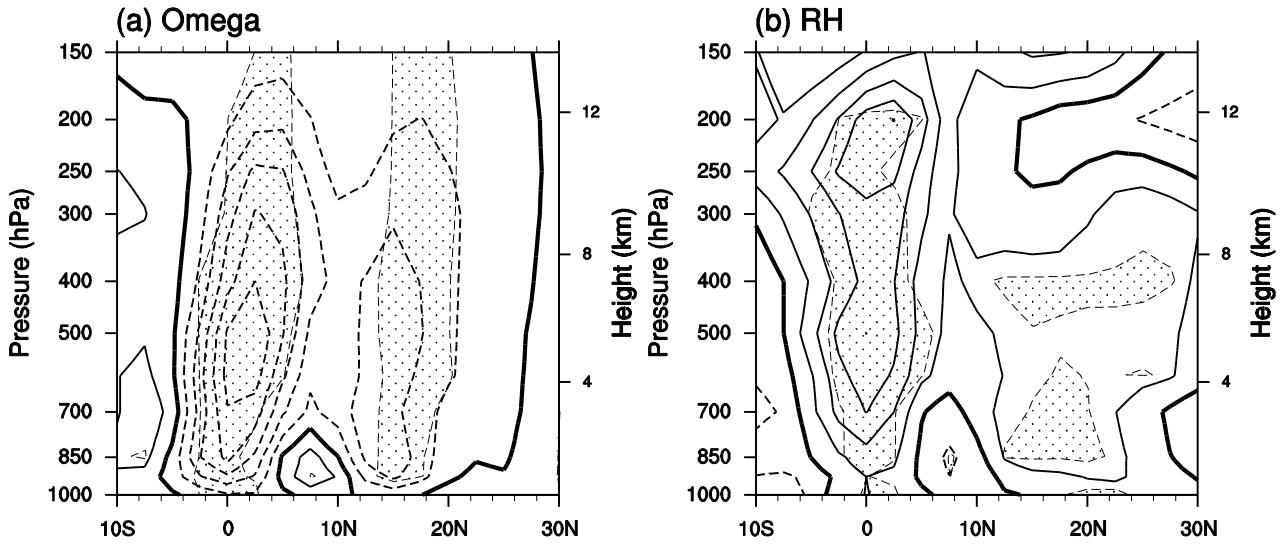

Figure 7. Composite differences of (a) omega (units: Pa s^{-1}; contour intervals: 5.0×10^{-3} Pa s^{-1}) and (b) relative humidity (units: %; contour intervals: 2%) averaged over 70°W-20°W. Zero lines are thickened, and solid (dash) lines indicate positive (negative) values. Shading indicates differences above the 95% confidence test.

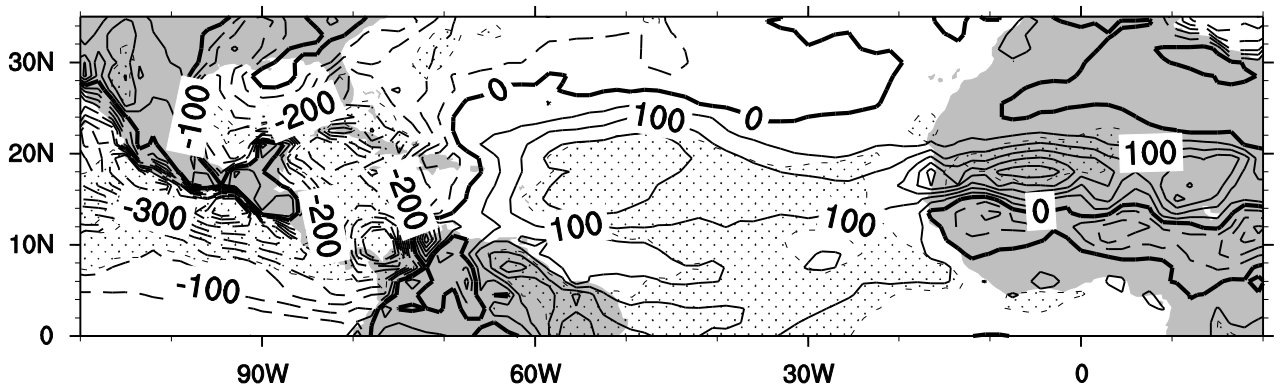

Figure 8. Composite difference of Convective Available Potential Energy (CAPE) (from ERA-Interim; contour intervals are 50 J kg^{-1}). Zero lines are thickened, and solid (dash) lines indicate positive (negative) values. Shading indicates differences above the 95% confidence test.

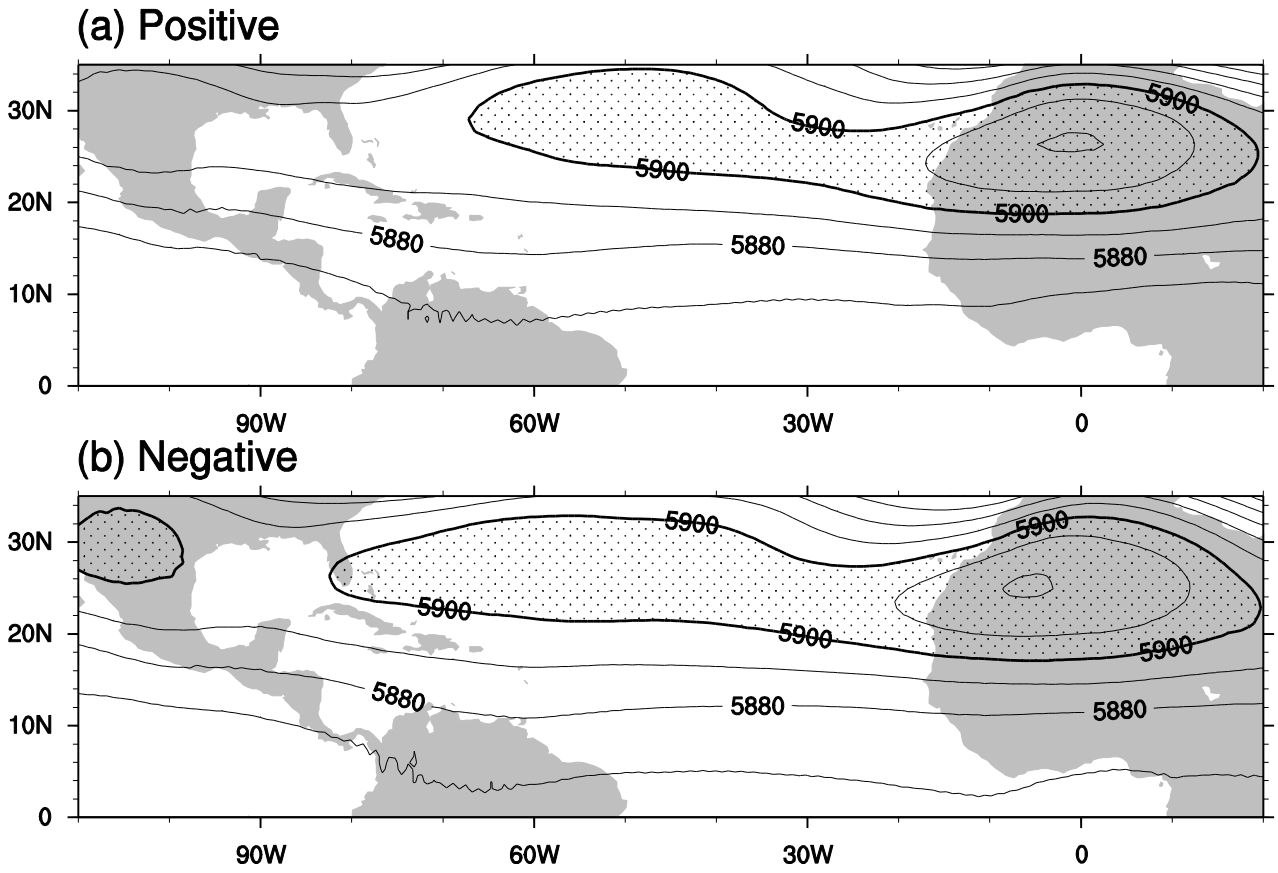

Figure 9. Composite mean of 500 hPa geopotential height for the (a) positive and (b) negative phases of M1. Values greater than 5900 gpm are highlighted in shading.

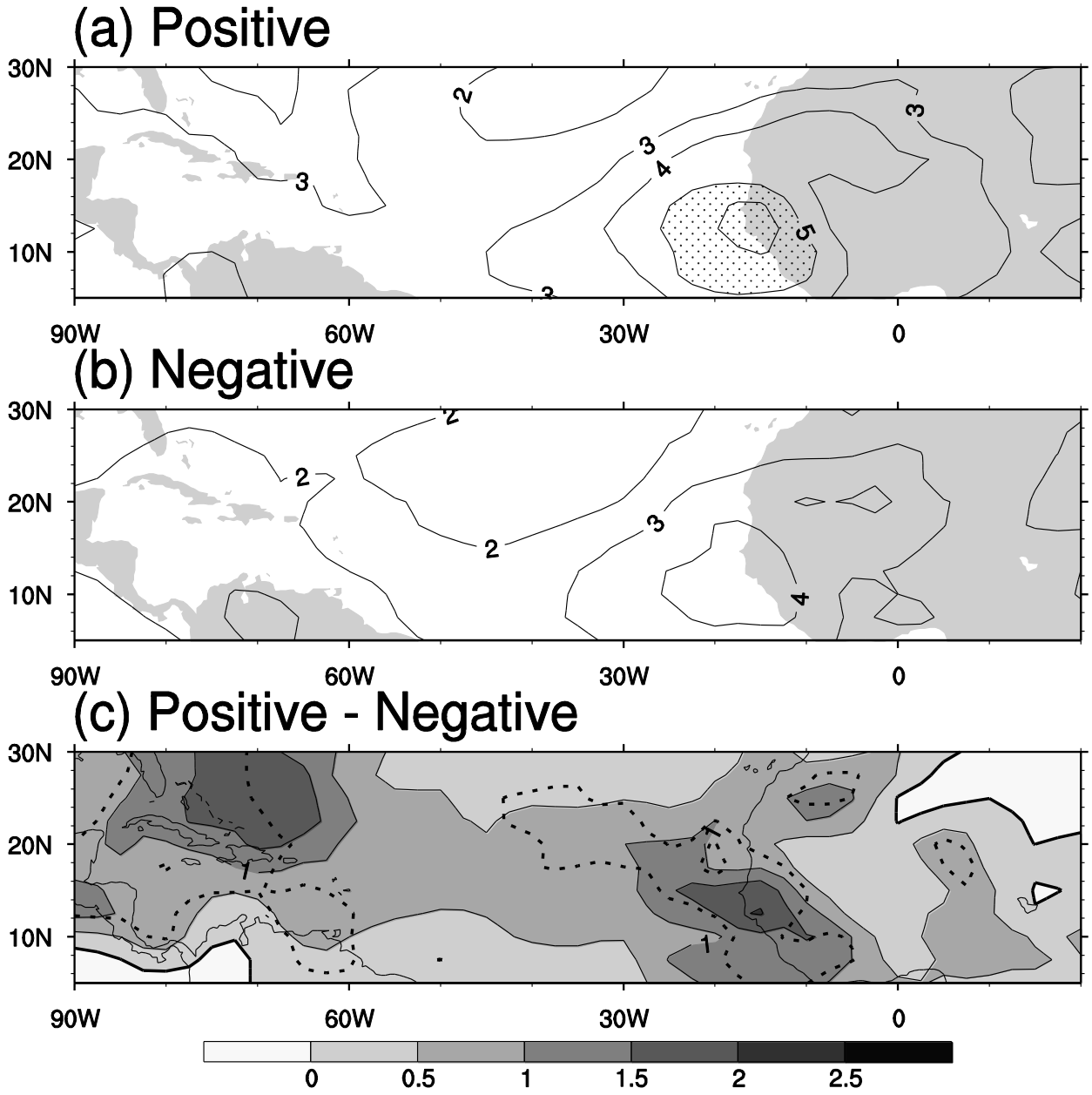

Figure 10. Eddy kinetic energy (units: $m^2 s^{-2}$) of 2.5 to 9-day band-pass filtered wind (850 hPa): the composite means for the (a) positive and (b) negative phases of M1, and (c) the composite difference. Values greater than 5 $m^2 s^{-2}$ are shaded. Dashed black line in (c) indicates the signal passes Student-t 95% confidence test.

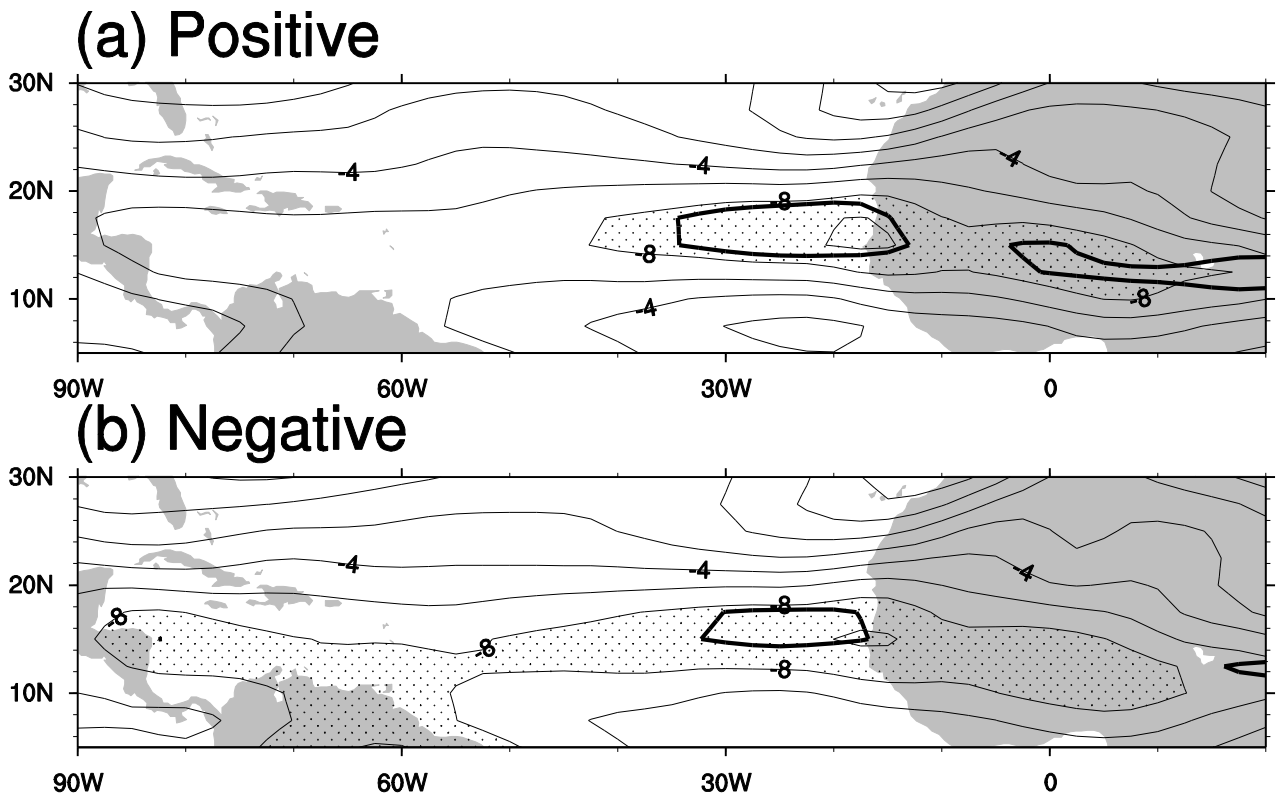

Figure 11. The composite means of the 700 hPa zonal wind (thin contours; values less than -8.0 m s^{-1} are shaded) for the (a) positive and (b) negative phases of M1. Thick black contour outlines the region where the meridional gradient of absolute vorticity (i.e., beta-U_{yy}) is negative.

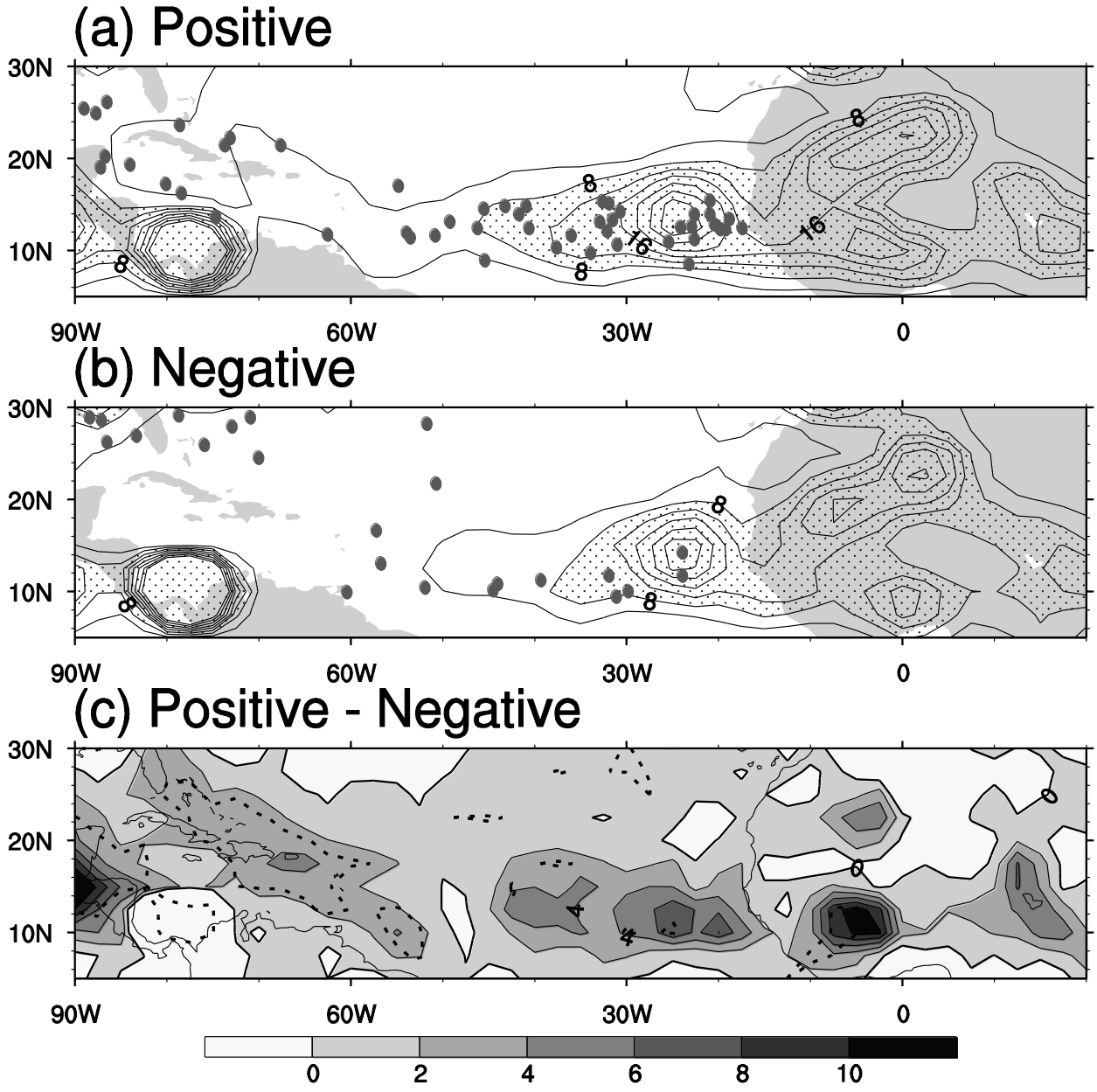

Figure 12. Wave Pouch Frequency (850 hPa) (units: days per season) for (a) the positive phase, (b) the negative phase and (c) the positive phase minus negative phase composites. The contour interval is 4 days per season in (a) and (b), and the contoured range is [0, 32]; values greater than 8 days per season are shaded. The black dots are the TC genesis locations in corresponding seasons. The dashed black line in (c) indicates the signal passes the 95% confidence test.

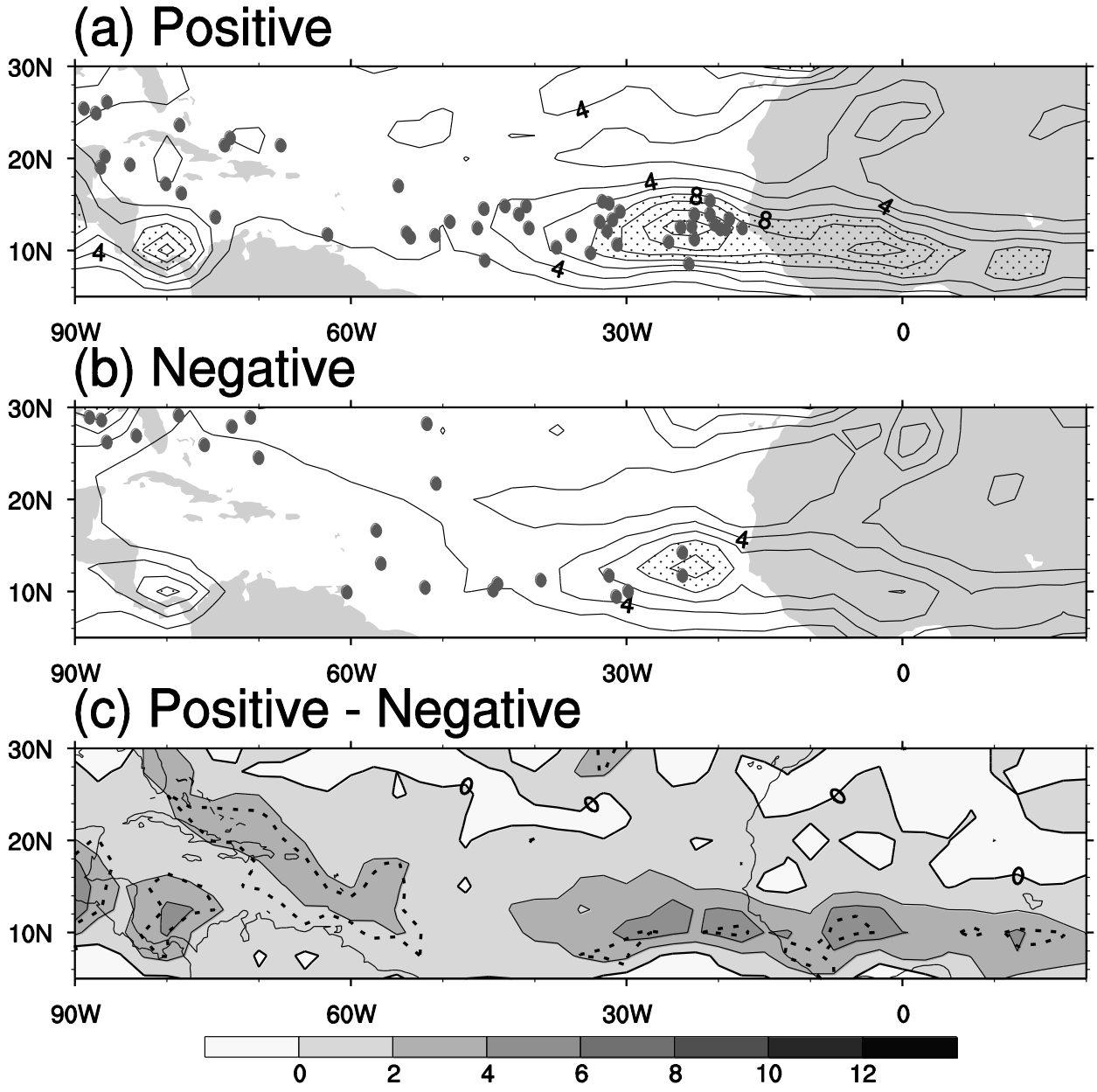

Figure 13. Same as Fig. 11, except for the frequency of vertically coherent wave pouches. The contour interval is 2 days per season in (a) and (b), and the contoured range is [0, 16].

REFERENCES

Adler, R. F., G. J. Huffman, A. Chang, R. Ferraro, P. Xie, J. Janowiak, B. Rudolf, U. Schneider, S. Curtis, D. Bolvin, A. Gruber, J. Susskind, P. Arkin, and E. Nelkin, 2003: The Version-2 Global Precipitation Climatology Project (GPCP) Monthly Precipitation Analysis (1979-Present). *J. Hydrometeor,* **4**, 1147-1167.

Arnault, J., F. Roux, 2011: Characteristics of African easterly waves associated with tropical cyclogenesis in the Cape Verde Islands region in July-August-September of 2004-2008. *Atmos. Res.,* **100**, 61-82.

Berry, G. J., C. Thorncroft, 2005: Case Study of an Intense African Easterly Wave. *Mon. Wea. Rev.*, **133**, 752–766.

Camara, A., A. Diedhiou, and A. Gaye, 2011: African Easterly Waves and Cyclonic Activity over the Eastern Atlantic: Composite and Case Studies. *International J. Geophys*, vol. 2011, Article ID 874292, 14 pages.

Chang, P., R. Saravanan, L. Ji, G. C. Hegerl, 2000: The Effect of Local Sea Surface Temperatures on Atmospheric Circulation over the Tropical Atlantic Sector. *J. Climate*, **13**, 2195–2216.

Chiang, J. C. H., Y. Kushnir, and A. Giannini (2002), Deconstructing Atlantic Intertropical Convergence Zone variability: Influence of the local cross-equatorial sea surface temperature gradient and remote forcing from the eastern equatorial Pacific, *J. Geophys. Res.*, **107**(D1), 4004.

Chiang, J. C. H., D. J. Vimont, 2004: Analogous Pacific and Atlantic Meridional Modes of Tropical Atmosphere–Ocean Variability. *J. Climate*, **17**, 4143–4158.

Colbert, A. J., B. J. Soden, 2012: Climatological Variations in North Atlantic Tropical Cyclone Tracks. *J. Climate,* **25**, 657-673.

Czaja, A., C. Frankignoul, 2002: Observed Impact of Atlantic SST Anomalies on the North Atlantic Oscillation. *J. Climate,* **15**, 606-623.

Davis, Christopher A., David A. Ahijevych, 2012: Mesoscale Structural Evolution of Three Tropical Weather Systems Observed during PREDICT. *J. Atmos. Sci.*, **69**, 1284–1305.

DeMaria, Mark, 1996: The Effect of Vertical Shear on Tropical Cyclone Intensity Change. *J. Atmos. Sci.*, **53**, 2076–2088.

Dima, I. M., J. M. Wallace, 2003: On the Seasonality of the Hadley Cell. *J. Atmos. Sci.*, **60**, 1522-1527.

Doblas-Reyes, Francisco J., Michel Déqué, 1998: A Flexible Bandpass Filter Design Procedure Applied to MidlatitudeIntraseasonal Variability. *Mon. Wea. Rev.*, **126**, 3326–3335.

Dunkerton, T. J., M. T. Montgomery, and Z. Wang, 2009: Tropical cyclogenesis in a tropical wave critical layer: easterly waves. *Atmos. Chem. Phys.*, **8**, 11149-11292.

Enfield, D. B., D. A. Mayer, 1997: Tropical Atlantic sea surface temperature variability and its relation to El Niño-Southern Oscillation. *J. Geophys. Res.*, **102**, 929-945.

Fang, J., and F. Zhang, 2010: Initial development and genesis of Hurricane Dolly (2008). *J. Atmos. Sci.*, 67, 655–672.

Fritz, C. L., and Z. Wang, 2012: A Numerical Study about the Impacts of Dry Air on Tropical Cyclone Formation. *J. Atmos. Sci.*, in press.

Goldenberg, S. B., C. W. Landsea, A. M. Mestas-Nuñez, and W. M. Gray, 2001: The recent increase in Atlantic hurricane activity: Causes and implications. *Science*, **293,** 474–479.

Gray, William M., 1968: Global View of The Origin of Tropical Disturbances and Storms. *Mon. Wea. Rev.*, **96**, 669–700.

Gray, W. M., 1984: Atlantic Seasonal Hurricane Frequency. Part I: El Niño and 30 mb Quasi-Biennial Oscillation Influences. *Mon. Wea. Rev.*, **112**, 1649–1668.

Gray, W. M., C. W. Landsea, 1992: African Rainfall as a Precursor of Hurricane-Related Destruction on the U.S. East Coast. *Bull. Amer. Meteor. Soc.*, **73**, 1352–1364.

Hopsch, S., C.D. Thorncroft, K. Hodges, and A. Aiyyer, 2007: West African storm tracks and their relationship to Atlantic tropical cyclones. *J. Climate*, **20**, 2468--2483

Hopsch, S. B., C. D. Thorncroft, and K. R. Tyle, 2010: Analysis of African Easterly Wave Structures and Their Role in Influencing Tropical Cyclogenesis. *Mon. Wea. Rev.*, **138**, 1399-1419.

Kanamitsu, M., W. Ebisuzaki, J. Woollen, S. Yang, J. J. Hnilo, M. Fiorino, and G. L. Potter, 2002: NCEP-DOE AMIP-II Reanalysis (R-2). *Bull. Amer. Meteor. Soc.*, **83**, 1631-1643.

Keenlyside, N., and M. Latif, 2007: Understanding Equatorial Atlantic Interannual Variability, *J. Climate*, **20**, 131-142.

Kossin, J. P., S. J. Camargo, and M. Sitkowski, 2010: Climate Modulation of North Atlantic Hurricane Tracks. *J. Climate*, **23**, 3057-3076.

Kossin, J. P., D. J. Vimont, 2007: A More General Framework for Understanding Atlantic Hurricane Variability and Trends. *Bull. Amer. Meteor. Soc.*, **88**, 1767-1781.

Landsea, C. W., 1993: A Climatology of Intense (or Major) Atlantic Hurricanes. *Mon. Wea. Rev.*, **121**, 1703-1713.

Landsea, C. W. , D. A. Glenn, W. Bredemeyer, M. Chenoweth, R. Ellis J. Gamache, L. Hufstetler, C. Mock, R. Perez, R. Prieto, J. Sanchez-Sesma, D. Thomas, and L. Woolcock, 2008: A Reanalysis of the 1911-20 Atlantic Hurricane Database. *J. Climate*, **21**, 2138-2168.

Landsea, C. W., W. M. Gray, 1992: The Strong Association between Western Sahelian Monsoon Rainfall and Intense Atlantic Hurricanes. *J. Climate*, **5**, 435–453.

Leroux, S., N. M. J. Hall, 2009: On the Relationship between African Easterly Waves and the African Easterly Jet. *J. Atmos. Sci.*, **66**, 2303–2316.

Lian, T., D. Chen, 2012: An Evaluation of Rotated EOF Analysis and Its Application to Tropical Pacific SST Variability. *J. Climate*, **25**, 5361–5373.

Lindzen, R. S., A. V. Hou, 1988: Hadley Circulations for Zonally Averaged Heating Centered off the Equator. *J. Atmos. Sci.*, **45**, 2416-2427.

Lübbecke, J. F., C. W. Böning, N. S. Keenlyside, and S.-P. Xie (2010), On the connection between Benguela and equatorial Atlantic Niños and the role of the South Atlantic Anticyclone, *J. Geophys. Res.*, **115**, C09015

Mitas, C. M., A. Clement, 2005: Has the Hadley cell been strengthening in recent decades? *Geophys. Res. Lett.,* **32**, L03809.

Montgomery, M. T., Wang, Z., and Dunkerton, T. J., 2010: Coarse, Intermediate and high resolution numerical simulations of the transition of a tropical wave critical layer to a tropical storm, *Atmos. Chem. Phys.*, **10**, 10803-10827.

Oort, Abraham H., James J. Yienger, 1996: Observed Interannual Variability in the Hadley Circulation and Its Connection to ENSO. *J. Climate*, **9**, 2751–2767.

Oort, Abraham H., Eugene M. Rasmusson, 1970: On the Annual Variation of the Monthly Mean Meridional Circulation. *Mon. Wea. Rev.*, **98**, 423–442.

Pytharoulis, Ioannis, Chris Thorncroft, 1999: The Low-Level Structure of African Easterly Waves in 1995. *Mon. Wea. Rev.*, **127**, 2266–2280.

Raymond, D. J., and C. Lo´pez Carrillo, 2011: The vorticity budget of developing Typhoon Nuri (2008). *Atmos. Chem. Phys.*, 11, 147– 163.

Reed, R. J., 1988: On understanding the meteorological causes of Sahelian drought. Persistent Meteo-Oceanographic Anomalies and Teleconnections, C. Chagas and G. Puppi, Eds., Pontificae Academiae Scientiarvm, 179–213.

Smirnov, D., D. J. Vimont, 2011: Variability of the Atlantic Meridional Mode during the Atlantic Hurricane Season. *J. Climate,* **24**, 1409-1424.

Smirnov, D., D. J. Vimont, 2012: Extratropical Forcing of Tropical Atlantic Variability during Boreal Summer and Fall. *J. Climate,* **25**, 2056-2076.

Smith, T. M., R. W. Reynolds, T. C. Peterson, and J. Lawrimore, 2008: Improvements to NOAA's Historical Merged Land-Ocean Surface Temperature Analysis (1880-2006). *J. Climate*, **21**, 2283-2296.

Stachnik, J. P., C. Schumacher, 2011: A comparison of the Hadley circulation in modern reanalyses. *J. Geophys. Res.*, **116**, D22102.

Sutton, R. T., D. L. R. Hodson, 2007: Climate Response to Basin-Scale Warming and Cooling of the North Atlantic Ocean. *J. Climate,* **20**, 891-907.

Swanson, K. L., 2008: Nonlocality of Atlantic tropical cyclone intensities, *Geochem. Geophys. Geosyst.*, 9, Q04V01.

Thorncroft, C., K. Hodges, 2001: African Easterly Wave Variability and Its Relationship to Atlantic Tropical Cyclone Activity. *J. Climate*, **14**, 1166-1179.

Thorncroft, C.D., Hall, N. and Kiladis, G., 2008: Three-dimensional structure and dynamics of African easterly waves: part III: Genesis, *J. Atmos. Sci.*, **65**, 3596-3607.

Ventrice, M. J., C. D. Thorncroft, M. A. Janiga, 2012: Atlantic Tropical Cyclogenesis: A Three-Way Interaction between an African Easterly Wave, Diurnally Varying Convection, and a Convectively Coupled Atmospheric Kelvin Wave. *Mon. Wea. Rev.*, **140**, 1108–1124.

Vimont, D. J., and J. P. Kossin, 2007: The Atlantic meridional mode and hurricane activity. *Geophys. Res. Lett.*, **34**, L07709,

Wang, Z., M. T. Montgomery, and T. J. Dunkerton, 2009: A dynamically-based method for forecasting tropical cyclogenesis location in the Atlantic sector using global model products. *Geophys. Res. Lett.*, **36**, L03801.

Wang, Z., M. T. Montgomery, and T. J. Dunkerton, 2010a: Genesis of Pre-hurricane Felix (2007). Part I: The Role of the Wave Critical Layer. *J. Atmos. Sci.*, **67**, 1711-1729.

Wang, Z., M. T. Montgomery, and T. J. Dunkerton, 2010b: Genesis of Pre-hurricane Felix (2007). Part II: Warm core formation, precipitation evolution and predictability. *J. Atmos. Sci.*, **67**, 1730-1744.

Wang, Z., M. T. Montgomery, and C. Fritz, 2012: A first look at the structure of the wave pouch during the 2009 PREDICT– GRIP dry runs over the Atlantic. *Mon. Wea. Rev.*, **140**, 1144– 1163.

Wang, Z., 2012: Thermodynamic aspects of tropical cyclone formation. *J. Atmos. Sci.*, **69**, 2433–2451.

Xie, Lian, Tingzhuang Yan, Leonard J. Pietrafesa, John M. Morrison, Thomas Karl, 2005: Climatology and Interannual Variability of North Atlantic Hurricane Tracks. *J. Climate*, **18**, 5370–5381.

Xue, Y., T. M. Smith, and R. W. Reynolds, 2003: Interdecadal changes of 30-yr SST normals during 1871-2000. *J. Climate*, **16**, 1601-1612.

Yin, X., A. Gruber, and P. Arkin, 2004: Comparison of the GPCP and CMAP Merged Gauge-Satellite Monthly Precipitation Products for the Period 1979-2001. *J. Hydrometeor*, **5**, 1207-1222.